Review of Scientific Instruments

Thin film lithium niobate electric field sensors

Cite as: Rev. Sci. Instrum. **93**, 034702 (2022); https://doi.org/10.1063/5.0080504
Submitted: 01 December 2021 • Accepted: 21 February 2022 • Published Online: 14 March 2022

Seyfollah Toroghi and Payam Rabiei

Review of Scientific Instruments ARTICLE scitation.org/journal/rsi

Thin film lithium niobate electric field sensors

Cite as: Rev. Sci. Instrum. 93, 034702 (2022); doi: 10.1063/5.0080504
Submitted: 1 December 2021 • Accepted: 21 February 2022 •
Published Online: 14 March 2022

Seyfollah Toroghi and Payam Rabiei[a)]

AFFILIATIONS

Partow Technologies LLC, 1487 Poinsettia Ave., Ste. 119, Vista, California 92081, USA

[a)]Author to whom correspondence should be addressed: pr@partow-tech.com

ABSTRACT

We present our results for using thin film lithium niobate devices for electric field sensing applications. Micro-ring modulator and Mach–Zehnder modulator-based electric field sensors are demonstrated. Micro-ring resonator sensors can be used for low frequency (up to several GHz) electric field sensing applications and achieve a high sensitivity of 80 mV/(m $Hz^{1/2}$) with a very compact size of 300 μm, as limited by the intensity and phase noise of the used distributed feedback laser. A measurement bandwidth of 2.5 GHz is measured for these sensors and is limited by the detector bandwidth. Alternatively, Mach–Zehnder modulators allow for perfect phase matching between the radio frequency signals and optical signals, and they can be used for electric field sensing up to several THz. A sensitivity of 2.2 V/(m $Hz^{1/2}$) was obtained using our Mach–Zehnder electric field sensor with an interaction length of 600 μm. The Mach–Zehnder sensor can sense electric fields with frequencies reaching 0.6 THz based on the calculated results.

I. INTRODUCTION

Electro-optic electric field (E-field) sensors are needed in many applications, such as antenna near-field characterization,[1] THz signal detection,[2] charged particle beam characterization in accelerators,[3] power grid monitoring,[4] and radio frequency (RF) ablation surgery. Electro-optic methods are among the best to measure E-fields, which cause a change in the refractive index of an electro-optic crystal. The change can then be detected by precise measurement equipment. Since an electro-optic material is a dielectric material, it does not perturb or scatter electromagnetic fields. Furthermore, because fiber optic cables are used to transmit the signal, any attached wiring does not pick up noise; hence, the probe can be used in a very noisy environment, and the measured signal is only related to the E-field at the probe location. Finally, the electro-optic response is extremely fast such that electro-optic field sensors can be used to modulate an optical signal and, thus, detect an electrical signal in the THz range.

Bulk whispering gallery mode ring resonator modulators and waveguide Mach–Zehnder modulators have been used to detect RF E-fields.[5,6] Optical ring resonators with a high quality factor can enhance sensor sensitivity, but the bandwidth (BW) of the measurement will be limited to that of the micro-ring resonator.[5] Waveguide Mach–Zehnder modulators have a higher bandwidth but are large and have a low spatial resolution.[6] Alternatively, bulk crystals can be used to measure an E-field, which are up to several mm long and can achieve sensitivity levels of 0.1 V/(m $Hz^{1/2}$).[7–9]

Thin film lithium niobate (TFLN) devices have been demonstrated recently for optical modulators, microwave frequency shifters, comb generation, and a variety of other photonic device functions. We present E-field sensors based on TFLN technology.[10]

The figure of merit for the sensitivity of E-field sensors with a given interaction length between the E-field and optical signals is proportional to r/ε, where r is the electro-optic coefficient and ε is the RF dielectric constant of the electro-optic material. For TFLN sensors, the effective RF dielectric constant is approximately equal to the substrate dielectric constant due to the small volume of the thin film layer compared to the substrate. The dielectric constant of quartz is smaller than that of lithium niobate by a factor of 20. Hence, by using TFLN waveguides on low-dielectric-constant substrates such as quartz, it is possible to achieve sensitivity levels that are significantly higher than bulk or waveguide-based sensors with the same interaction length.

In addition, TFLN sensors allow for phase matching between THz signals and optical signals.[11] Previously, modulation speeds as high as THz have been achieved experimentally using phase-matched TFLN waveguide modulators.[12] In a TFLN platform, the effective index for a THz signal is almost equal to the SiO_2 (or quartz substrate) refractive index (~2 at a wavelength of 1550 nm) and is not affected by the submicrometer-thick TFLN. This index is close

to the effective refractive index of the optical guided mode propagating through a TFLN waveguide. Hence, it is easier to achieve phase matching between a THz signal and an optical signal. Free-space TFLN modulators can then be used to characterize the THz free-space signals.

Finally, using TFLN technology, more complex sensors, such as waveguide micro-ring resonators, can be fabricated. This simultaneously achieves a small size and high sensitivity, which are required for many novel applications of E-field sensors, such as microwave ablation surgery or electronic circuitry inspection equipment. In this paper, we review the results of micro-ring and Mach–Zehnder sensors fabricated using TFLN technology.

II. DEVICE STRUCTURES

A Mach–Zehnder modulator, a micro-ring structure, and a Mach–Zehnder Interferometer Coupled Ring structure (MZICR), as shown in Figs. 1(a)–1(c), respectively, are three different device structures used as electro-optic E-field sensors. All the structures are fabricated by etching the device into a TFLN that is bonded to a quartz substrate, which are fiber-coupled to an integrated photonic chip that has grating couplers to couple the light from the optical fiber to a sub-micrometer lithium niobate optical waveguide on the chip.

For the Mach–Zehnder device structure, the coupled light is divided between two arms of a Mach–Zehnder interferometer using a 1 × 2 multimode interference (MMI) coupler device. One arm of the Mach–Zehnder interferometer is poled to reverse the direction of spontaneous polarization of the lithium niobate crystal. Hence, for one arm, the refractive index increases for a given E-field, while it decreases for the same E-field for the other arm. Thus, the phase of the light that is passing through the two arms is modulated in opposite directions. The output MMI coupler combines these two phase-modulated signals and produces an intensity-modulated signal. While the bandwidth of Mach–Zehnder E-field sensors based on the bulk lithium niobate structure is limited to 20 GHz,[6] the Mach–Zehnder structure based on our TFLN structure can be used to sense E-fields reaching several THz. Using TFLN waveguide technology, it is possible to engineer phase matching between the propagating THz signal and an optical wave. A modulation bandwidth reaching 10 THz can be achieved theoretically, and modulation speeds close to 1 THz have been shown experimentally.[12] The frequency-dependent transfer function of an electro-optical modulator can be determined by

$$T_{RF} = \frac{\sin(\omega_{RF}(n_{RF} - n_o)l/2c)}{\omega_{RF}(n_{RF} - n_o)l/2c},$$

where l, ω_{RF}, n_{RF}, and n_o are the length of the electro-optical modulator, the RF frequency, the RF refractive index, and the optical refractive index, respectively. For the non-optimum phase-matched devices using a lithium niobate thickness of 600 nm that we are currently producing, the normalized modulation response $|T_{RF}|^2$ as a function of modulation frequency is shown in Fig. 2 for different lengths of the device. Using our current 600-μm-long device, the theoretical bandwidth is close to 600 GHz.

For micro-ring structures, two types of devices are produced. Figure 1(b) shows a simple ring structure coupled to the waveguide.

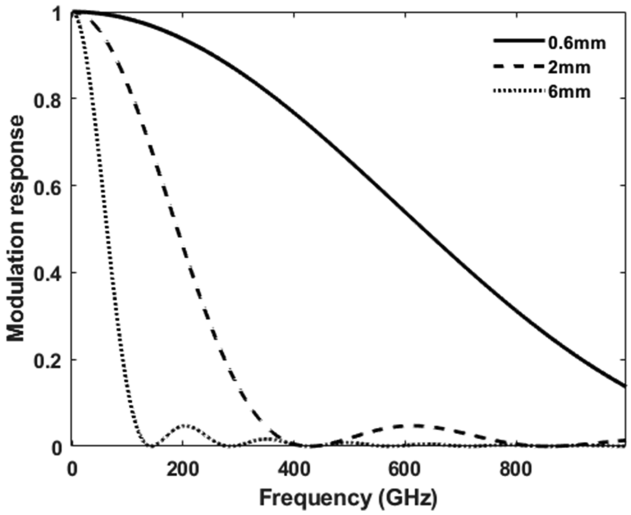

FIG. 2. Calculated modulation bandwidth for TFLN (thickness of 600 nm) modulators with different device arm lengths.

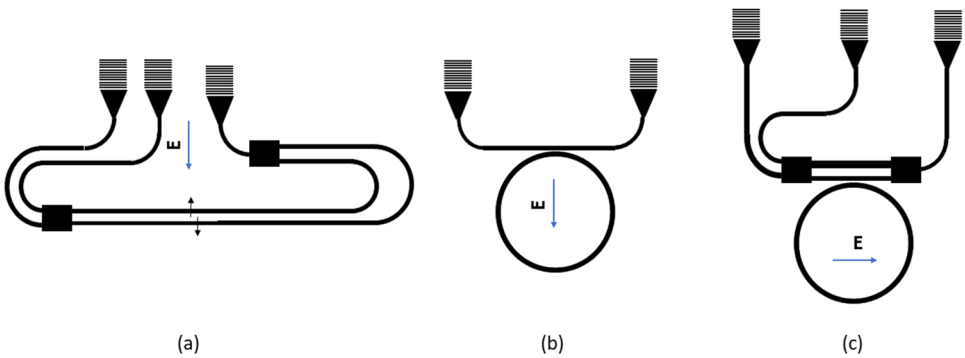

FIG. 1. Schematics of (a) Mach–Zehnder E-field sensor, (b) micro-ring resonator sensor, and (c) Mach–Zehnder interferometer coupled micro-ring resonator.

The gap is optimized to achieve critical coupling. The laser wavelength is adjusted close to the resonance wavelength of the device to achieve the highest modulation signal. No poling is needed for the micro-ring-type device, which simplifies its fabrication. Alternatively, one can use a MZICR device, where its laser wavelength is adjusted to that of the resonator. The E-field causes a modulation in phase that is converted to an intensity-modulated signal by the Mach–Zehnder interferometer structure. For the MZICR-type device, not only one can obtain a slightly higher sensitivity but also a balanced detection scheme can be used to reduce noise. In addition, controlling the laser wavelength to match the resonance of the resonators is easier compared to simple micro-ring devices since two outputs are available. However, all the resonance-based devices have an inherent limitation in the modulation bandwidth, which is approximately equal to the resonator linewidth.

III. FABRICATION PROCESS

The fabrication flow for our optical Mach–Zehnder modulators based on the TFLN platform is shown in Fig. 3.[10,13] The TFLN platform is achieved by transferring a thin layer of lithium niobate onto a quartz substrate using the crystal ion slicing method, as shown in Figs. 3(a) and 3(b). A bulk lithium niobate crystal is ion implanted and bonded to a quartz substrate. A subsequent heating process transfers a thin layer of lithium niobate to the quartz substrate. The transferred single crystalline TFLN has the same optical and electro-optical properties as the bulk lithium niobate crystals. After producing TFLN, electrodes are placed onto the sample for a subsequent poling process, as shown in Figs. 3(c) and 3(d). The device is then poled for Mach–Zehnder-type sensors using a high-voltage power supply, where selective arms of the Mach–Zehnder sensor are poled, as shown in Fig. 3(d). In order to pole the device, it is immersed in silicone oil, and an E-field higher than the coercive field of lithium niobate (~22 kV/mm) is applied to the sample. Figure 4 shows a typical poling current that passes through the device. The electrodes are then removed. In the next step, the optical circuit of the sensor is patterned using electron beam lithography and is formed by dry-etching the lithium niobate layer, as shown in Fig. 3(e). The fabrication steps seen in Figs. 3(c) and 3(d) are omitted

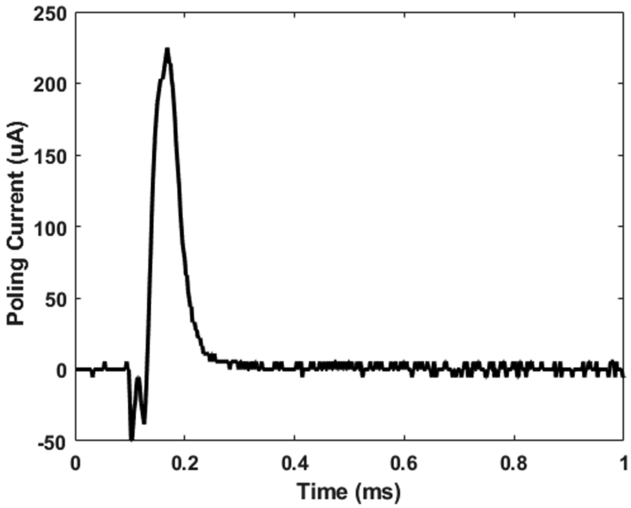

FIG. 4. Typical poling current passing through the device.

for the fabrication of ring resonator sensors, where the device structure is etched into the lithium niobate layer without any electrodes or poling process. Fiber-optic v-groove arrays are subsequently aligned and attached to the device to achieve a fiber-coupled device structure. More details on the fabrication process and device structures are explained in Ref. 10.

IV. DEVICE CHARACTERIZATIONS

A. Ring-resonator electro-optic E-field sensor

Figure 5(a) shows an image of a fabricated and packaged micro-ring resonator-based E-field sensor. As can be seen, the packaged sensor is very compact. Current packaged devices are as large as 3×3 mm^2. However, unpackaged devices can be designed such that the entire device is as small as the diameter of the fiber (i.e., 250 μm). A fiber-to-fiber insertion loss of 13 dB is obtained for micro-ring resonators and Mach–Zehnder modulators [see Fig. 5(b)]. Figure 5(c)

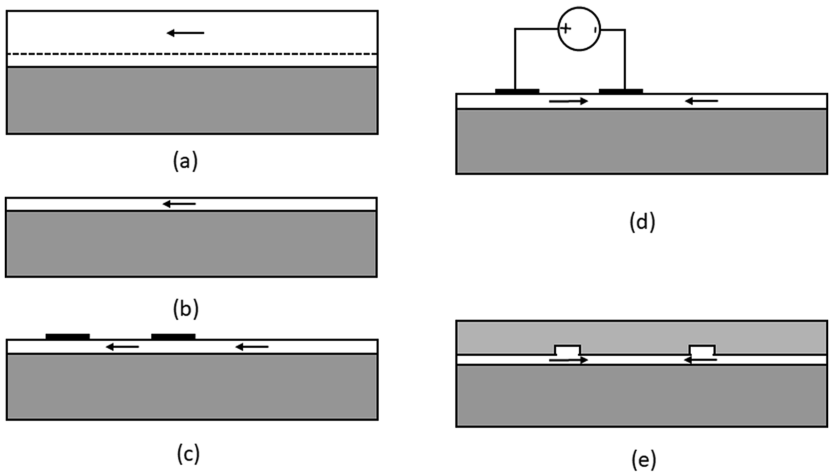

FIG. 3. Fabrication process steps to produce the Mach–Zehnder sensor chip based on TFLN. (a) Ion implantation and bonding of the lithium niobate crystal to a quartz substrate. Dashed lines represent the ion implanted layer of the lithium niobate layer. (b) Crystal ion slicing process and TFLN production. (c) Poling electrode deposition. (d) High voltage poling process. (e) Electron beam lithography, etching, waveguide formation, and polymer passivation layer deposition. Arrows indicate the direction of spontaneous polarization of the TFLN layer.

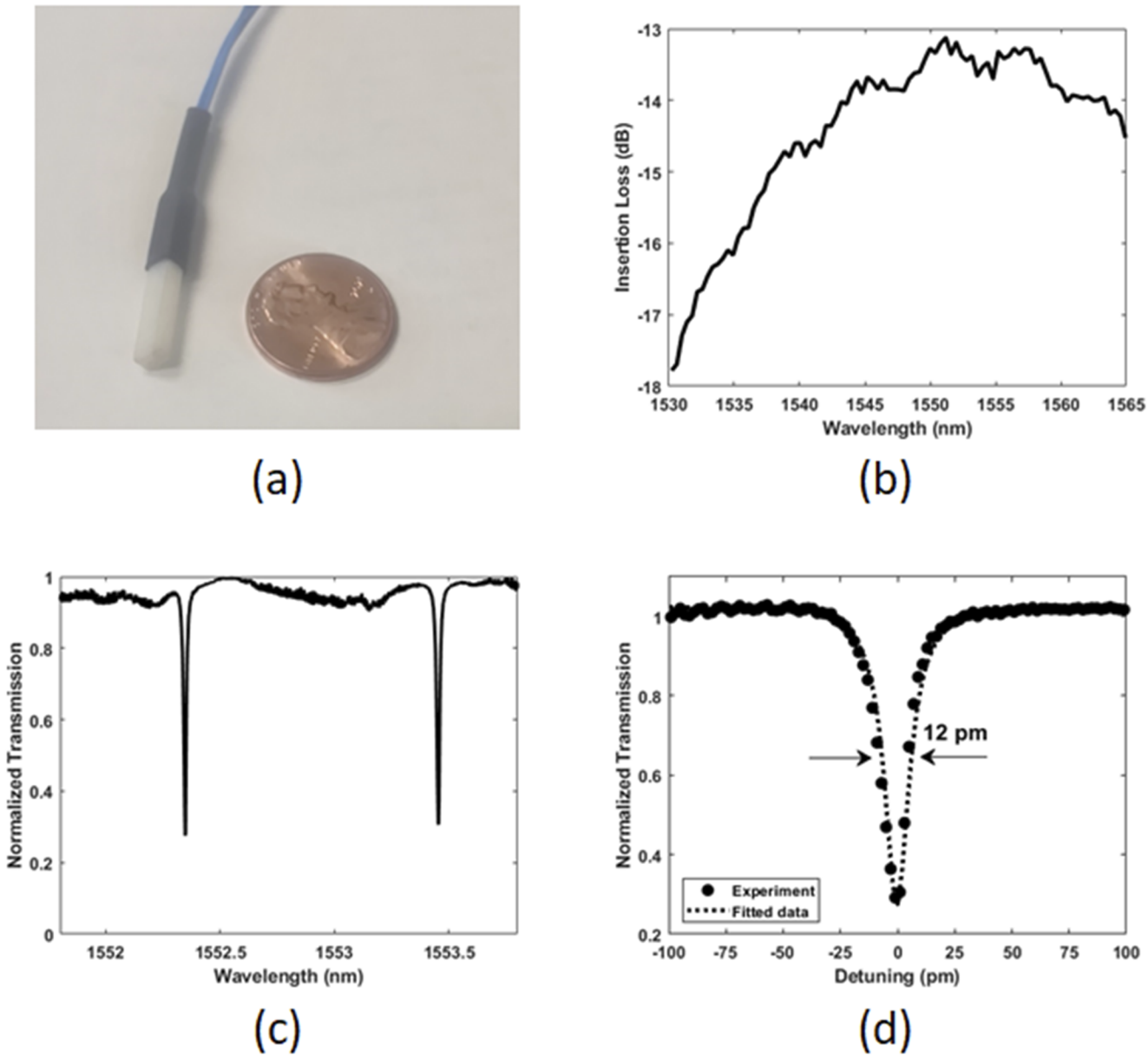

FIG. 5. (a) Packaged electric field sensor head, (b) measured insertion loss for the grating coupler (after passing two input and output couplers), (c) normalized transmission of the fabricated ring resonator on TFLN, and (d) fitted data to calculate the propagation loss of the waveguide.

shows the optical transmission of a fabricated ring resonator. The ring resonator has a quality factor of 1.2×10^5 with a linewidth of 12 pm (1.5 GHz) and a calculated propagation loss of 2.5 dB/cm [see Fig. 5(d)]. A lower insertion loss of 0.1 dB/cm can be achieved with an improved fabrication process that results in better sensitivity. However, since the resonance will be narrower, it will limit the operational bandwidth of the device and will require a very narrow laser linewidth in order to achieve higher sensitivity, since any phase noise will convert to intensity noise after the micro-ring resonator device. Using this technology, a sensitivity level of 5 $mV/mHz^{0.5}$ with a maximum bandwidth of ~300 MHz is expected.

Figure 6 shows the sensitivity measurement results for a micro-ring resonator sensor, where a fiber-attached ring resonator was placed inside a parallel plate capacitor that provided a uniform E-field. A function generator was used to apply a sinusoidal bias of 100 kHz and 12 V to the capacitor plates. The spacing of the capacitor plate was set at 14 mm. We used a low-cost distributed feedback (DFB) laser, where temperature tuning was

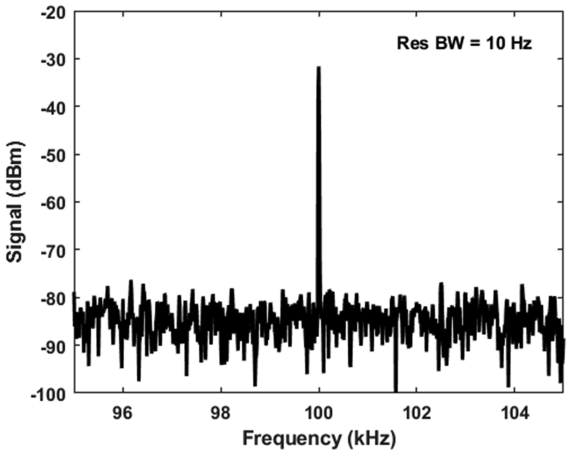

FIG. 6. Measured response of an E-field ring resonator sensor for 12 V sinusoidal applied voltage at 100 kHz with an electrode gap of 14 mm.

performed to lock the wavelength of the laser to the resonance wavelength of the resonator. The output power of the laser was 12.7 dBm, and a detector with a conversion gain of 40 000 V/W was used. Figure 6 shows the measured signal using an electrical spectrum analyzer. A −31 dBm signal was measured with a noise floor of −86 dBm. Considering the resolution Bandwidth (BW) of 10 Hz of the spectrometer, the sensitivity of the sensor was 180 mV/(m $Hz^{1/2}$).

Figure 7(a) shows the measured transmission spectrum of MZICR. The highest sensitivity is achieved at the resonance wavelength for this type of sensor. The measured sensitivity of this sensor using a spectrum analyzer was 80 mV/(m $Hz^{1/2}$). An improvement in sensitivity of a factor of 2 has been achieved using MZICR structures. In addition, dual output allows one to use a balanced detection scheme, which, in turn, leads to significantly easier control and the ability to lock the resonance wavelength to the laser wavelength for this type of sensor. Using measured signals from a balanced detector and a feedback loop, we adjusted the laser wavelength to track the resonance shift due to small temperature variations. Thus, we could

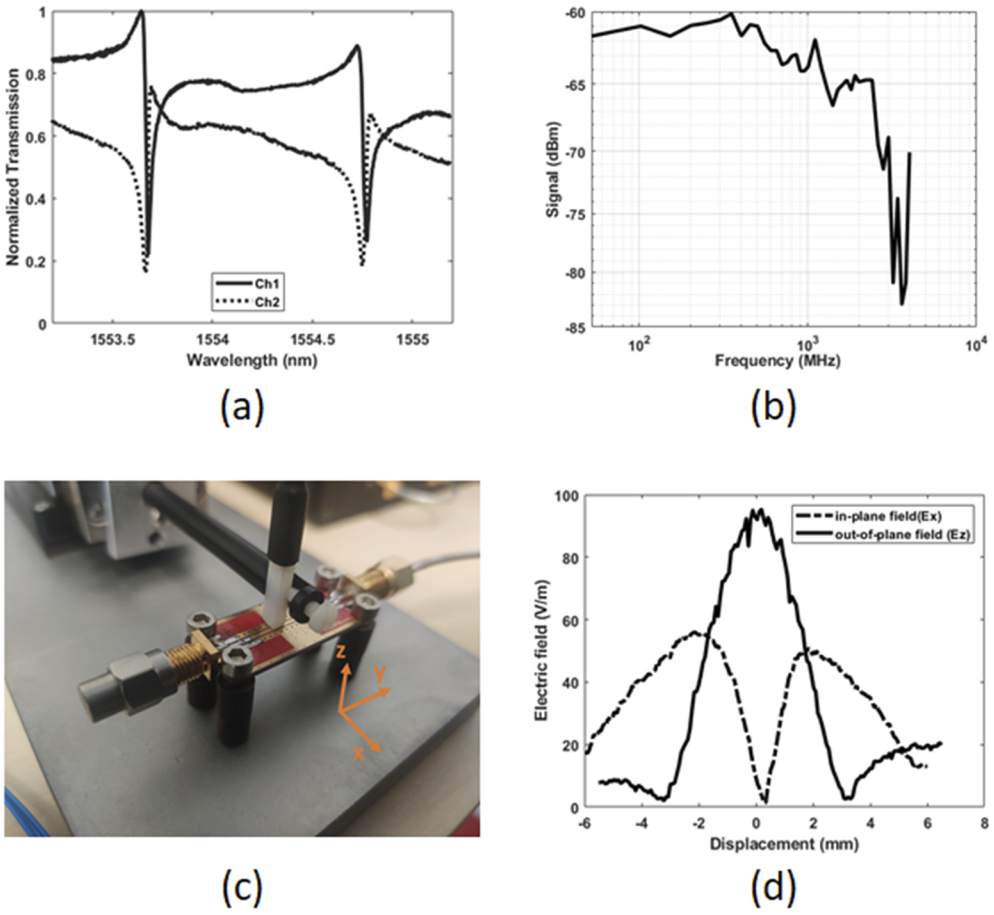

FIG. 7. (a) Measured transmission spectrum, (b) measured frequency response of a MZICR resonator structure device, (c) measurement setup for high-frequency characterization of the sensor, and (d) measured in-plane and out-of-plane electric field vs displacement of the sensor with respect to the transmission line.

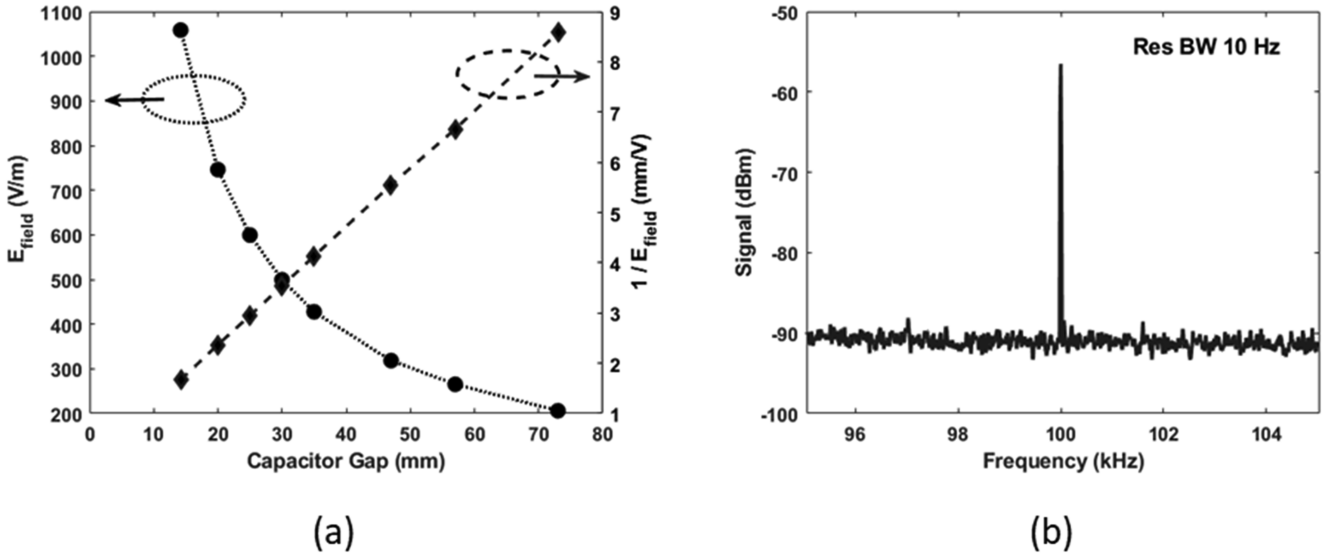

FIG. 8. (a) Measured electric field vs capacitor gap (circles) and inverse of the measured electric field vs capacitor gap (diamonds) for a Mach–Zehnder E-field sensor for a 12-V sinusoidal signal at 100 kHz. (b) Measured response of a Mach–Zehnder E-field sensor for 12-V sinusoidal applied voltage at 100 kHz for 20 mm gap.

easily control the laser wavelength using a simple feedback loop for the MZICR structure.

Figure 7(b) shows the measured frequency response of a MZICR device using an RF signal generator and measuring the E-field on top of a coplanar transmission line, as shown in Fig. 7(c). The RF power in this measurement was 23 dBm. The coplanar transmission line was terminated in a 50-Ω resistor. The device had a flat frequency response up to 2.5 GHz, and the bandwidth of the detector used in this measurement was 2.5 GHz. Therefore, the signal drop at 2.5 GHz was related to the bandwidth of the detector and not the device.

Figure 7(d) shows the measured E-field as a function of probe spatial location with respect to transmission lines. Different components of the E-fields were measured as the sensor was displaced on top of the coplanar transmission line using the micrometer stage. The results of measurements match theory and good spatial resolution were obtained.

The sensitivities of these sensors are on par with other technologies using several-mm-long interaction lengths. The ring structure is a very compact sensor, and it can be used for applications simultaneously requiring high sensitivity and high spatial resolution, such as medical procedures, plasma characterization, and printed circuit board electromagnetic compatibility measurements.

B. Mach–Zehnder EO E-field sensor

Using a poled Mach–Zehnder structure, shown in Fig. 1(a), we fabricated and tested E-field sensors. The device was placed inside an E-field using a parallel plate capacitor as previously described. A function generator was used to apply a 100-kHz, 12-V, sinusoidal voltage to the capacitor plates. The spacing of the capacitor plate was set to change from 14 to 73 mm. The laser power was set at 12.7 dBm. A balanced detector with a gain of 40 000 V/W was used. Figure 8(a) shows the measured signal as the applied sinusoidal E-field changes by increasing the gap between the parallel plate capacitors, as well as the measured signal for a 20-mm gap. The signal was inversely linearly proportional (with a bias) to the separation between the electrodes. The bias was due to slight changes that happen in the field of the parallel plate capacitor due to loading effects from the dielectric constant of the sensor. Figure 8(b) shows the measured signal using a spectrum analyzer for an applied sinusoidal E-field of 600 V/m, where a −56 dBm signal was measured with a noise floor of −92 dBm. Considering the resolution bandwidth (BW) of 10 Hz for the spectrometer, the sensitivity of the sensor was calculated to be as low as 2.2 V/(m $Hz^{1/2}$), with an estimated bandwidth of 600 GHz. We have tested the functionality of the sensor between 0 and 100 °C, and the response and the sensitivity of the sensor are not affected by the temperature change in that range.

V. CONCLUSION

Electro-optical electric field sensors based on TFLN have been designed, fabricated, and characterized. Two types of electric field sensors, the ring resonator and Mach–Zehnder types, have been investigated. The platform includes a dry etched lithium niobate rib section on top of a slab layer of lithium niobate on a quartz substrate. The fabricated devices are packaged using fiber v-groove arrays, where each grating coupler has an insertion loss of 6.5 dB. Sensitivities of 80 and 2.2 V/(m $Hz^{1/2}$) were measured for the MZICR resonator and Mach–Zehnder types, respectively.

ACKNOWLEDGMENTS

We acknowledge the support from a phase I DOE SBIR project (Contract No. DE-SC0019625).

AUTHOR DECLARATIONS

Conflict of Interest

The authors have no conflicts to disclose.

DATA AVAILABILITY

The data that support the findings of this study are available from the corresponding author upon reasonable request.

REFERENCES

[1]G. Gaborit, P. Artillan, C. Bermond, G. Revillod, G. Chevrier-Gros, and L. Duvillaret, IEEE Antennas Wireless Propag. Lett. **19**(7), 1177 (2020).
[2]C. Winnewisser, P. U. Jepsen, M. Schall, V. Schyja, and H. Helm, Appl. Phys. Lett. **70**, 3069 (1997).
[3]Y. K. Semertzidis, V. Castillo, L. Kowalski, D. E. Kraus, R. Larsen, D. M. Lazarus, B. Magurno, D. Nikas, C. Ozben, T. Srinivasan-Rao, and T. Tsang, Nucl. Instrum. Methods Phys. Res., Sect. A **452**, 396 (2000).
[4]C. Volat, M. Jabbari, M. Farzaneh, and L. Duvillaret, IEEE Trans. Dielectr. Electr. Insul. **20**(1), 194 (2013).
[5]A. A. Savchenkov, W. Liang, V. S. Ilchenko, E. Dale, E. A. Savchenkova, A. B. Matsko, D. Seidel, and L. Maleki, AIP Adv. **4**, 122901 (2014).
[6]S. S. Sriram and S. A. Kingsley, Proc. SPIE **5435**, 143 (2004).
[7]L. Duvillaret, S. Rialland, and J.-L. Coutaz, J. Opt. Soc. Am. B **19**(11), 2692 (2002).
[8]G. Gaborit, J.-L. Coutaz, and L. Duvillaret, Appl. Phys. Lett. **90**(24), 241118 (2007).
[9]M. Bernier, G. Gaborit, L. Duvillaret, A. Paupert, and J.-L. Lasserre, Appl. Opt. **47**(13), 2470 (2008).
[10]P. Rabiei, J. Ma, S. Khan, J. Chiles, and S. Fathpour, Opt. Express **21**, 25573 (2013).
[11]J. Rollinson, M. Hella, S. Toroghi, P. Rabiei, and I. Wilke, J. Opt. Soc. Am. B **38**, 336 (2021).
[12]A. J. Mercante, S. Shi, P. Yao, L. Xie, R. M. Weikle, and D. W. Prather, Opt. Express **26**(11), 14810 (2018).
[13]P. Rabiei, "Electro-optic optical modulator devices and method of fabrication," U.S. patent 9746743B1 (29 August 2017).